ELSEVIER

International Journal of Pharmaceutics 151 (1997) 109–119

international journal of pharmaceutics

Rigorous analysis of S_2L-type phase solubility diagrams to obtain individual formation and solubility product constants of both SL-and S_2L-type complexes

M.B. Zughul [a], A.A. Badwan [b,*]

[a] *Department of Chemistry, University of Jordan, Amman, Jordan*
[b] *The Jordanian Pharmaceutical Manufacturing Company, PO Box 94, 11710 Naor, Jordan*

Received 10 October 1996; revised 13 January 1997; accepted 27 January 1997

Abstract

A rigorous simple model has been developed for the analysis of S_2L-type phase solubility diagrams. The model utilizes the inherent information built into all segments of the phase diagram to obtain individual formation (K_{11} and K_{21}) and solubility product constants, either K_{S11} or K_{S21}, depending on which of the two SL or S_2L complexes reaches saturation first. The model uses the measured solubility S_{eq} against solubiliser concentration L_t, in addition to the corresponding values at the onset and end of the plateau. This is used to analyze the entire phase diagram including the descending portion. Nonlinear least square fitting of the entire data sets proved quite efficient in converging to a unique fit, especially because the model includes only one single floating parameter to estimate. The model offers a simple vehicle to distinguish between the two types of S_2L phase solubility profiles: those involving an S_2L-complex precipitate, and others having an SL-complex precipitate instead. The limits of precision required to obtain reasonable estimates of formation constants were investigated through computer simulation of experimental data. © 1997 Elsevier Science B.V.

Keywords: S_2L-type complexes; Inclusion complexes; Formation constants; Phase solubility diagrams; Solubilization

1. Introduction

Phase solubility techniques have extensively been utilized to examine the extent of solubility enhancement exerted by some water-soluble compounds on certain water-insoluble materials (Higuchi and Connors, 1965; Uekama et al., 1980; Seo et al., 1983; Muller and Brauns, 1985; Duchene and Wouessidjewe, 1990; Marques et al., 1990; Menard et al., 1990; Sideris et al., 1992). Analysis of the variation of solubility of the solute

* Corresponding author. Tel.: +962 6 727207; fax: +962 6 727641; e-mail: jpm@go.com.jo

PII S0378-5173(97)04901-6

(substrate, S) against the stoichiometric concentration of the solubiliser (ligand, L) provides information on the type of solute-solubiliser complexes formed in solution. This may offer some insight into the type of chemical interactions taking place and hence facilitate more understanding of possible mechanisms underlying complex formation.

A large number of the phase solubility diagrams reported in literature show a rising portion, which may or may not be linear, followed by a horizontal plateau, and a descending portion indicating a fall in the solubility with increase in solubiliser concentration. Attempts of analysis of phase diagrams have largely been directed at the rising portion which is often insufficient to establish the type of complexes formed in solution (Connors et al., 1982, 1988; Connors and Pendergast, 1984; Streng et al., 1984; Takahashi et al., 1986; Hoshino et al., 1988; Liu et al., 1990; Valsami et al., 1990; Abdul Rasool et al., 1991; Yusuff and York, 1991; Tong et al., 1991; Maurin et al., 1994; Krishnamoorthy and Mitra, 1996). This is particularly evident in most systems where the rising portion of the diagram appears rather linear and hence only allows the determination of what is commonly called the *apparent formation constant* K.

Individual formation constants may, however, be obtained from the descending portions of phase diagrams which, by virtue of their nonlinearity, provide more information. Scanning the scientific literature reveals a relatively large number of phase solubility diagrams belonging to solute-solubiliser systems forming S_2L-, SL- and/or SL_2- type soluble complexes (Connors et al., 1982, 1988; Connors and Pendergast, 1984; Streng et al., 1984; Takahashi et al., 1986; Hoshino et al., 1988; Liu et al., 1990; Valsami et al., 1990; Tong et al., 1991; Maurin et al., 1994; Krishnamoorthy and Mitra, 1996). Those S_2L-type phase diagrams showing a plateau followed by a descending portion may further be classified into systems precipitating either SL- or S_2L-type complexes, depending on which of the two complexes reaches saturation first due to its relative lower solubility. As to SL_2-type phase diagrams, they may similarly be classified into those precipitating either SL- or SL_2-type complexes beyond saturation.

Each case requires a different set of relations to obtain the individual formation constants. These systems will be separately dealt with in order to establish rigorous yet simple models for analysis of all segments of the phase diagram. These models will be tested for consistency through computer simulation to check their validity. Furthermore, statistical random noise will be superimposed on simulated data in order to establish the appropriate limits of precision required to obtain reasonable estimates of formation constants. This article will mainly be concerned with those phase diagrams belonging to solute-solubiliser systems forming S_2L-type complexes. Both cases where either an S_2L-complex reaches saturation first, or an SL-complex reaches saturation while the higher order S_2L-complex remains soluble will be addressed.

2. Theoretical background

The equilibria involved in solute-solubiliser systems forming S_2L-type complexes are:

$$S + L \Leftrightarrow SL, \qquad [SL] = K_{11} \cdot [S] \cdot [L] \tag{1}$$

$$S + SL \Leftrightarrow S_2L, \qquad [S_2L] = K_{21} \cdot [S] \cdot [SL] \tag{2}$$

where K_{11} and K_{21} are the partial formation constants of SL and S_2L-complexes, respectively. The molar concentrations of various soluble solute and solubiliser species are then defined in terms of the equilibrium stoichiometric concentrations of solute (S_{eq}) and solubiliser (L_{eq}) for each region of the phase diagram. For convenience and to utilize all the information provided by the entire phase diagram resulting from an S_{eq} versus L_t plot, it has been segmented into three regions: region I depicting the rising portion, region II denoting the horizontal plateau, and region III corresponding to the descending portion as depicted in Fig. 1. The curve labeled region IV represents how the data of regions II and III appear in an S_{eq} versus L_{eq} plot.

2.1. Region I

Referring to the rising portion of the phase diagram shown in Fig. 1, the solute is present in excess at equilibrium with soluble species and thus the free solute concentration is fixed at $[S] = S_o$. The equilibrium stoichiometric concentrations are then given through mass balance by

$$S_{eq} = [S] + [SL] + 2\cdot[S_2L]$$
$$= S_0 + K_{11}\cdot S_0(1 + 2\cdot\delta)[L] \quad (3)$$

$$L_{eq} = [L]\cdot\{1 + K_{11}\cdot S_0(1 + \delta)\} = L_t \quad (4)$$

where

$$\delta = K_{21}S_0 \quad (5)$$

and L_t is the initial stoichiometric concentration of solubiliser species in solution. The slope of the rising portion of the phase diagram (region I) is therefore given as

$$T = K_{11}\cdot S_0(1 + 2\cdot\delta)/\{1 + K_{11}\cdot S_0(1 + \delta)\} \quad (6)$$

The two unknown parameters in this relation are K_{11} and K_{21} can only be determined from a nonlinear least square analysis of the data corresponding to the descending portion of the phase diagram (region III) as will be shown later. It is useful however to examine the effect of the relative K_{21}/K_{11} value on the magnitude of the slope T. This may become more obvious when Eq. (6) is cast in the following form

$$T = \{K_{11}\cdot S_0\cdot\delta + K_{11}\cdot S_0(1 + \delta)\}$$
$$/\{1 + K_{11}\cdot S_0(1 + \delta)\} \quad (7)$$

Comparison of the numerator with the denominator of Eq. (7) reveals that the slope T may assume values within the following three ranges for various S_2L-type solute-solubiliser systems, namely:

a. $T < 1$ if $K_{11}\cdot S_0\cdot\delta < 1$ or

$$K_{21} < (K_{11}S_0^2)^{-1} \quad (8)$$

b. $T = 1$ if $K_{11}\cdot S_0\cdot\delta = 1$ or

$$K_{21} = (K_{11}S_0^2)^{-1} \quad (9)$$

c. $T > 1$ if $K_{11}\cdot S_0\cdot\delta > 1$ or

$$K_{21} > (K_{11}S_0^2)^{-1} \quad (10)$$

The most commonly encountered solute-solubiliser systems belong to case 'a' above, including those forming only SL-type complexes for which $K_{21} = 0$. Though we presently have no knowledge of systems exhibiting case 'b' or case 'c' behaviours, they cannot be ruled out and the present analysis would be equally applicable.

For the purpose of later use and evaluation of K_{11} and δ, Eq. (7) may be conveniently rearranged into either of the following forms:

$$K_{11}(1 + \delta) = (T - K_{11}\cdot S_0\delta)/\{S_0(1 - T)\} \quad (11)$$

$$K_{11} = \{(T - K_{11}\cdot S_0\delta)\}/\{S_0(1 - T)(1 + \delta)\} \quad (12)$$

$$K_{11} = T/\{S_0(1 - T + \delta(2 - T))\} \quad (13)$$

Either of the three forms may equally be used to obtain the first estimate (guess) of K_{11} in a nonlinear least square analysis of data of region III by setting $\delta = 0$. The form depicted in Eq. (11), however, looks more familiar in estimating the so called *apparent formation constant* K, and this is commonly obtained from the slope of the rising portion of the phase diagram by ignoring the term $K_{11}\cdot S_o\ \delta$ in the numerator to yield

$$K = K_{11}(1 + \delta) \approx T/\{S_0(1 - T)\} \quad (14)$$

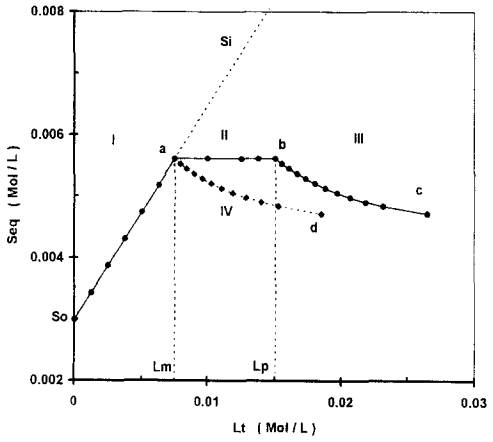

Fig. 1. Phase solubility diagram for an S_2L/S_2L-precipitate system having the parameter values: $S_o = 0.003$ M, $S_m = 0.00562$ M, $L_m = 0.00834$ M, $L_p = 0.00159$ M, $[L_m] = 0.006$ M, $K_{11} = 25.00\ M^{-1}$, $K_{21} = 800.0\ M^{-1}$, $K_{S21} = 5.4 \times 10^{-7}\ M^3$ and $S_t = 0.02067$ M. Region IV is a plot of the equilibrium stoichiometric concentration of solute S_{eq} against L_{eq}.

2.2. Region II

This region represented by a horizontal plateau in an S_{eq} versus L_t plot occurs due to the onset of precipitation of either an SL or an S_2L complex, whichever is less soluble, while the solution is still saturated with excess solute species. Thus depending on which of the two complexes reaches saturation first, there are two separate cases to consider:

(a) The solution is saturated with an S_2L-complex which begins precipitating subject to the constraint on S_t and L_t given by

$$S_t > \{S_m + 2\cdot(L_t - L_m)\}; \qquad L_t > L_m \tag{15}$$

where L_m is the stoichiometric equilibrium concentration of the solubiliser species at S_m; both of which obtained from the intersection of regions I and II of the phase diagram.

(b) The solution is saturated with an SL-complex instead which begins to precipitate subject to the constraint

$$S_t > \{S_m + (L_t - L_m)\}; \qquad L_t > L_m \tag{16}$$

In either case, the molar concentrations of free solute [S] and free solubiliser [L] species remain fixed at $[S] = S_o$ and $[L] = [L_m]$ and thus the concentrations of all other soluble species are also fixed at

$$[SL]_m = K_{11}\cdot S_0\cdot[L_m] = \text{constant} \tag{17}$$

$$[S_2L]_m = K_{11}\cdot S_0\cdot\delta[L_m] = \text{constant} \tag{18}$$

This corresponds to an invariant system represented by a single data point on an S_{eq} vs L_{eq} plot corresponding to point a in Fig. 1 whose coordinates (S_m, L_m) are given by:

$$S_m = S_0 + [SL]_m + 2\cdot[S_2L]_m \tag{19}$$

$$L_m = [L_m] + [SL]_m + [S_2L]_m \tag{20}$$

and thus the free solubiliser concentration is given by

$$[L_m] = L_m/\{1 + K_{11}\cdot S_0\cdot(1+\delta)\} \tag{21}$$

2.3. Region III

The solubility of the solute begins to decrease in this region because the insoluble complex continues precipitating at the expense of free solute species. This occurs as a result of having the initial amount of solute S_t insufficient to maintain the free solute concentration fixed at S_o as in regions I and II. There are two separate cases to consider depending on which of the two complexes precipitates in region II and continues on precipitating in region III:

2.3.1. S_2L-complex precipitate

An S_2L-complex continues on precipitating subject to the constraints on S_t and L_t given by

$$S_m < S_t < \{S_m + 2\cdot(L_t - L_m)\}; \qquad L_t > L_m \tag{22}$$

Note that S_t may or may not be larger than the solubility expected from the rising portion of the phase diagram S_I at L_t depending on the relative magnitudes of the individual formation constants K_{11} and K_{21}, and hence on the slope T. The magnitude of S_I corresponding to solubiliser stoichiometric concentration L_t is obtained from Eq. (3) according to

$$S_I = S_0 + K_{11}\cdot S_0(1 + 2\cdot\delta)[L] \tag{23}$$

where [L] is the concentration of free solubiliser species corresponding to L_t as defined through Eq. (4) by

$$[L] = L_t/\{1 + K_{11}\cdot S_0(1+\delta)\} \tag{24}$$

Since excess S_2L will be at equilibrium with soluble species, its concentration in solution would be fixed at the same value of region II and hence the free solute concentration [S] decreases as the free solubiliser concentration [L] increases subject to the condition

$$[S_2L] = [S_2L]_m = K_{11}\cdot S_0\cdot\delta[L_m] \tag{25a}$$

or

$$[S]^2\cdot[L] = S_0^2\cdot[L_m] = K_{S21} \tag{25b}$$

and thus $[S] < S_o$ while

$$[L] = S_0^2\cdot[L_m]/[S]^2 > [L_m] \tag{26}$$

K_{S21} is the solubility product of S_2L-complex, and the equilibrium stoichiometric concentrations of solute and solubiliser in solution would be given by

$$S_{eq} = [S]\cdot(1 + K_{11}\cdot[L]) + 2\cdot[S_2L]_m \quad (27)$$

$$L_{eq} = [L]\cdot(1 + K_{11}\cdot[S]) + [S_2L]_m \quad (28)$$

Substituting for $[S_2L]_m$ from Eq. (25a) and for [L] from Eq. (26) into Eq. (28), rearranging, and solving for [S] leads to

$$[S] = \{b + (b^2 + 4\cdot a\cdot c)^{1/2}\}/2\cdot a \quad (29)$$

$$[L] = c/[S]^2 \quad (30)$$

where $a = (L_{eq} - K_{11}\bullet S_o\bullet[L_m])$, $b = K_{11}\bullet c$, $c = S_0^2\cdot[L_m]$ and $[L_m]$ is given by Eq. (21).

There is only one floating variable δ to be determined here from a nonlinear least square fitting of the experimentally measured quantities S_{eq} and L_{eq} for region III. The fitting procedure is initiated by setting the first guess for the parameter δ which is $\delta = 0$. This is followed by estimating each of the following quantities in the sequence: K_{11}, $[L_m]$, [S] and [L] from Eqs. (13), (21), (29) and (30), respectively. Finally, the predicted equilibrium stoichiometric concentration of solute species for each data point is calculated according to:

$$S^p_{eq} = [S]\cdot(1 + K_{11}\cdot[L]) + 2\cdot[S_2L]_m \quad (31)$$

Nonlinear least square fitting to obtain the best value for δ (subject to the constraint $\delta \geq 0$) is then started by minimizing the sum:

$$Q = \Sigma(S_{eq} - S^p_{eq})^2 \quad (32)$$

Once δ is estimated, the partial formation constants K_{21} and K_{11} are calculated from Eqs. (5) and (13), respectively. Following that the molar concentrations of all soluble species can be computed and thus a complete chemical speciation over the entire three regions of the phase diagram is arrived at.

Note that the equilibrium stoichiometric concentration of solubiliser species L_{eq}, if not directly measured, is given by

$$L_{eq} = L_t - (L_p - L_m) - 0.5\cdot(S_m - S_{eq}) \quad (33)$$

where L_p is the equilibrium stoichiometric concentration of the solubiliser at the intersection of regions II and III.

2.3.2. SL-complex precipitate

An SL-complex continues on precipitating at the expense of free solute species subject to the constraints on S_t and L_t given by

$$S_m < S_t < \{S_m + (L_t - L_m)\}; \qquad L_t > L_m \quad (34)$$

Again, since solid SL remains at equilibrium with solution, its soluble concentration remains fixed at the same value of region II, such that both [S] and [L] vary subject to the condition

$$[SL] = [SL]_m = K_{11}\cdot S_0\cdot[L_m] = K_{11}K_{S11} \quad (35)$$

or

$$[S]\cdot[L] = S_0\cdot[L_m] = K_{S11} \quad (36)$$

where K_{S11} is the solubility product of SL-complex and thus it follows that [S] decreases below S_o while [L] rises according to

$$[S] = S_0\cdot[L_m]/[L] \quad (37)$$

The equilibrium stoichiometric concentrations of solute and solubiliser in solution would be given by

$$S_{eq} = [S]\cdot(1 + 2\cdot K_{21}\cdot[SL]_m) + [SL]_m \quad (38)$$

$$L_{eq} = [L] + [SL]_m(1 + K_{21}\cdot[S]) \quad (39)$$

Substituting for $[SL]_m$ from Eq. (35) and for [S] from Eq. (36) into Eq. (39), rearranging and solving for [L] leads to

$$[L] = 0.5\cdot\{b_1 + (b_1^2 - 4\cdot a_1)^{1/2}\} \quad (40)$$

where $a_1 = (K_{11}\bullet K_{S11})^2K_{21}$, $b_1 = L_{eq} - K_{11}\bullet K_{S11}$, while L_{eq} is given by:

$$L_{eq} = L_t - (L_p - L_m) - (S_m - S_{eq}) \quad (41)$$

As [S] and [L] are given by Eqs. (37) and (40), the equilibrium solute concentration S^p_{eq} is computed and the rest of the analysis is conducted exactly as discussed earlier by minimizing the sum of squares of errors defined by Eq. (32).

3. Simulation results and discussion

Fig. 1 depicts a typical phase solubility diagram obtained for a solute-solubiliser system forming an S_2L-type complex which begins to precipitate

following saturation. The phase diagram was constructed bearing the following parameter values: $S_o = 0.003$ M, $S_m = 0.00562$ M, $L_m = 0.00834$ M, $L_p = 0.00159$ M, $[L_m] = 0.006$ M, $K_{11} = 25.00$ M^{-1}, $K_{21} = 800.0$ M^{-1}, $K_{S21} = 5.4 \times 10^{-7}$ M^3 and $S_t = 0.02067$ M. The diagram shows the solubility S_{eq} rising linearly with L_t which happens to be equal to L_{eq} for region I (line S_o to a). Since the solute is in excess of its optimal solubility at the plateau ($S_t > S_m$), the free solute concentration remains fixed at $[S] = S_o$ while [L] keeps rising linearly with L_t to its plateau value $[L_m]$ given by Eq. (21). The slope of the line $T = 0.346614$ is given by Eq. (6) and thus yields an apparent formation constant $K = 176.8293$ according to Eq. (14).

Region II (line a–b) of Fig. 1 appears as a horizontal plateau since the S_2L-type complex begins to precipitate at equilibrium with its soluble species. The solute is also present at S_t in excess of S_m, and this results in fixing [S] and [L] at S_o and $[L_m]$, respectively. Thus the concentrations of all soluble species ([S], [L], [SL] and $[S_2L]$) remain fixed and the equilibrium stoichiometric concentrations S_{eq} and L_{eq} become fixed at S_m and L_m, respectively.

Region III (curve b–c) occurs once S_t becomes insufficient to maintain the free solute concentration at S_o (Eq. (22)), the complex continues on precipitating at the expense of free solute concentration [S], while [L] increases subject to the constraint of Eq. (26).

The segment of the phase diagram depicted as region IV (curve a–d) in Fig. 1 represents how regions II and III appear in a plot of S_{eq} against L_{eq} given by Eq. (33).

The procedure followed in applying the set of relations described earlier for the analysis of the entire phase diagram for S_2L- and SL-precipitate systems is illustrated as follows.

Fig. 2(a) is a reproduction of the three regions of the same phase diagram shown in Fig. 1. Linear least square fitting of region I yields S_o and T. Since Fig. 2(a) represents precise data with no statistical random noise superimposed onto it, both input values are recovered as they are listed in the second column of Table 1. The fact that the slope of this line $T < 1$ allows estimation of the

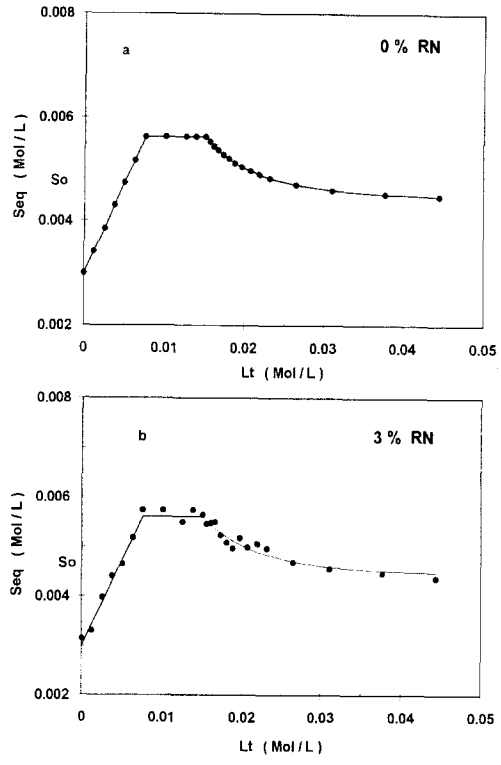

Fig. 2. A plot showing the result of nonlinear least square fitting of the entire phase diagram shown in Fig. 1 with a single floating parameter δ. (a) No random noise have been superimposed, while (b) random noise have been superimposed to the extent of 3% of the optimal solubility S_m. In either case, the solid line represents the least square fit.

commonly used *apparent formation constant* K according to Eq. (14). This also establishes the relation between K_{11} and K_{21} through T and δ governed by Eq. (5) and Eq. (13), respectively. Next, S_m and L_m are both determined from the intersection of regions I and II, and L_p from the intersection of regions II and III. Following that, nonlinear least square fitting of the entire data is initiated by setting $\delta = 0$, calculating first estimates of K_{11} according to Eq. (13), [L] for region I according to Eq. (24), setting $[S] = S_o$ and $[L_m]$ from Eq. (21) for region II, and finally [L], [S] and L_{eq} for region III from Eqs. (26), (29) and (33), respectively. This is followed by computing S^p_{eq} according to Eq. (31), the sum of squares of errors Q according to Eq. (32) and the least square routine is started. The only constraint

Table 1
Retrieved parameter estimates following nonlinear least square fitting of the entire S_2L-type phase diagram with an S_2L-complex precipitate using an initial guess of $\delta = 0$

Parameter	Input data	% Random noise superimposed					
		0%	1%	2%	3%	4%	5%
S_o (M) (% error)	0.003000	0.003000	0.002999	0.003032	0.003001	0.002982	0.002925
(% error)		(0.000)	(0.33)	(1.07)	(0.03)	(0.60)	(2.50)
S_m (M)	0.00562	0.00562	0.00563	0.005551	0.005626	0.005607	0.005739
(% error)		(0.000)	(0.18)	(1.23)	(0.11)	(0.23)	(2.12)
T	0.346614	0.346081	0.346081	0.338973	0.349622	0.352802	0.368383
(r)		(0.99998)	(0.99984)	(0.99954)	(0.99748)	(0.99754)	(0.99827)
K (M^{-1})	176.8293	176.8292	176.4726	169.1285	179.1294	182.8042	199.3976
(% error)		(0.0)	(0.26)	(4.35)	(1.30)	(3.38)	(12.8)
δ	2.400000	2.400531	2.369396	2.400054	2.45379	2.380004	2.384885
(% error)		(0.022)	(1.28)	(0.23)	(2.24)	(0.83)	(0.63)
K_{11} (M^{-1})	25.00000	24.99525	25.23643	24.05519	24.78732	23.81267	27.846
(% error)		(0.02)	(0.95)	(3.78)	(0.85)	(4.75)	(11.4)
K_{21} (M^{-1})	800.0000	800.177	790.0619	791.1285	817.6573	879.7305	815.3453
(% error)		(0.022)	(1.24)	(1.11)	(2.21)	(9.97)	(1.92)

applied to the floating parameter δ is $\delta \geq 0$. It has been found that convergence was attained after 7 to 11 trials (iterations) using either PC statistical packages: SPSS/PC + Version 5.0 (SPSS Inc., 444 N. Michigan Avenue, Chicago, Illinois 60611), or the SOLVER Statistical Tool built into Microsoft Excel spreadsheet, Version 5.0. The results of the fitting procedure after retrieving the best value of δ are listed in the third column of Table 1 for data having no statistical noise, and in columns 5–9 for 1%, 2%, 3%, 4% and 5% (of the optimal solubility S_m) random noise separately superimposed onto the solubility S_{eq}. Fig. 2(b) depicts a typical fitted data set corresponding to 3% random noise for comparison with that of Fig. 2(a).

Inspection of Table 1 shows that all parameters may be retrieved with percent error reasonably well within 4 to 5% (95% confidence level) providing random noise does not exceed 3% of S_m. Beyond that the percent error in parameter estimates may well surpass 5% particularly for K_{11}, K_{21} and of course δ. Although the % error in S_o and S_m are relatively low, the precision with which they can be determined has a significant effect on those of the formation constants since errors add up. The absence of a systematic trend in the percent error of retrieved parameters with % random noise is due to the fact that random noise was separately generated for each data set, and thus was not fixed for all.

Fig. 3(a) is a phase diagram constructed with the same input parameters of Fig. 2 except for having an SL-complex precipitate instead. The solubility product K_{S11} was set equal to 1.8×10^{-5} M^2 in order to retain an identical behavior except for the descending portion of the phase diagram. The procedure followed in fitting the data sets to retrieve estimates of the parameters is the same except for those of region III where [S], [L] and L_{eq} are computed according to Eqs. (37), (40) and (41), respectively. Next, both S^P_{eq} and Q are computed as before and the minimizing routine is started. Again, convergence was attained promptly to provide the best estimate of δ from which the formation constants are estimated. The results of data fitting are listed in Table 2 which retains the same parameter estimates of region I and II as for those of Table 1 except for having both S_o and S_m fixed at their input values. The same random noise sets were used in both cases to simplify comparison.

As is seen in Table 2, the formation constants were retrieved to better than 5% error up to 4% random noise. The % errors in δ and K_{21} are the

same since S_o was fixed for all data sets at 0.003 M. There appears a tendency for retrieval of a slightly higher estimate of K_{11} as opposed to a corresponding lower estimate of K_{21} as the % random noise increases. Fig. 3(b) shows a typical data fit for 3% random noise compared with that of 0% random noise in Fig. 3(a). The quality of the fitting procedure appears quite good keeping in mind that the number of data points $n = 28$ for the entire phase diagram. Therefore it is expected that the error in parameter estimates will rise in proportion to $n^{-1/2}$ as n decreases.

Several trials were conducted to check whether it was possible to fit an S_2L-type phase diagram with an S_2L-complex precipitate (i.e. Fig. 2) to

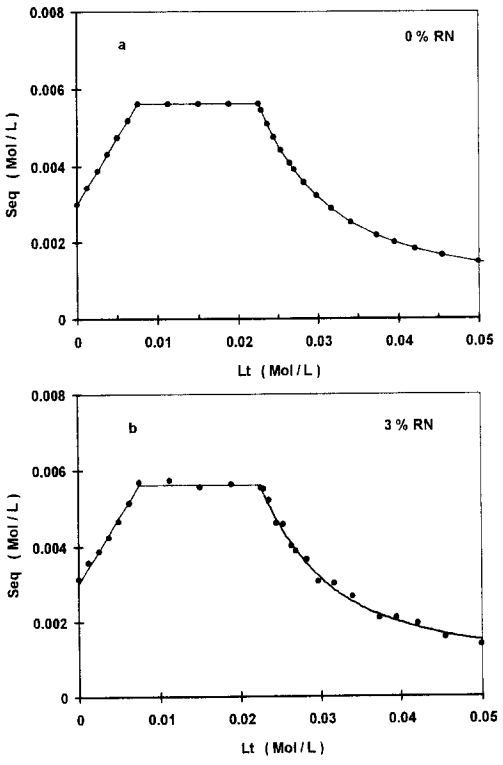

Fig. 3. A plot showing the result of nonlinear least square fitting of the entire phase diagram for an S_2L/SL-precipitate system having the same parameter values used in Fig. 2 except for $K_{S11} = 1.8 \times 10^{-5}$ M^2 with a single floating parameter δ. (a) No random noise have been superimposed, while (b) random noise have been superimposed to the extent of 3% of the optimal solubility S_m. Again, the solid line represents the least square fit.

S_2L-type with an SL-complex precipitate, and vice versa. Fortunately, it was found impossible to achieve convergence in either case since the fitting routine halts while searching for a minimum in Q, and this made it possible to ensure that convergence was unique each time it was applied.

Fig. 4 presents several phase solubility diagrams constructed for an S_2L/S_2L-precipitate system as opposed to Fig. 5 which depicts the corresponding phase diagrams for an S_2L/SL-precipitate system. The sets of formation constants used in both cases are one-to-one duplicates with the same S_o value retained for ease of comparison.

In Fig. 4, the slope of region I increases as the magnitudes of K_{11}, K_{21} and K_{11}/K_{21} ratio increase from diagram c up to a while keeping the product $K_{11} \cdot K_{21}$ constant. For a given complex system, the width of the plateau is only a function of the initial amount of solute added, S_t, increasing as L_t increases. The height of the plateau increases only as the solubility product K_{S21} increases. The general shape of the descending portion of the phase diagram is a combined function of the four parameters K_{11}, K_{21}, K_{S21} and S_t with the extent of curvature decreasing as S_t increases. It is interesting to note that at higher magnitudes of K_{11}, K_{21} and K_{11}/K_{21} ratio and higher S_t, keeping the product $K_{11} \cdot K_{21}$ constant, region III begins to flip over towards higher solubility. This may explain the earlier observation for some systems of a rise following a decrease in solubility which was unnecessarily attributed to possible onset of formation of higher order complexes (Higuchi and Connors, 1965). The slope of region I of diagram d is low enough to lie flat along with region II due to low values of K_{11}, K_{21} and K_{S21} which may also explain the appearance of some phase diagrams without a rising portion within experimental uncertainty (Higuchi and Connors, 1965). The lowest phase diagram (e in Fig. 4) corresponds to a system having relatively low values of K_{11}, K_{21} and S_t to the extent where both regions I and II almost disappear.

Fig. 5 depicts phase diagrams corresponding to an S_2L/SL-precipitate system which show the same trends for regions I and II as before since the same magnitudes of formation constants, S_o and S_m were retained. The difference, however,

Table 2
Retrieved parameter estimates following nonlinear least square fitting of the entire S_2L-type phase diagram with an SL-complex precipitate using an initial guess of $\delta = 0$

Parameter	Input data	% Random noise superimposed					
		0%	1%	2%	3%	4%	5%
S_o (M)	0.003000	0.003000	0.003000	0.003000	0.003000	0.003000	0.003000
S_m (M)	0.00562	0.00562	0.00562	0.00562	0.00562	0.00562	0.00562
T	0.346614	0.346081	0.346081	0.338973	0.349622	0.352802	0.368383
(r)		(0.99998)	(0.99984)	(0.99954)	(0.99748)	(0.99754)	(0.99827)
K (M^{-1})	176.8293	176.8292	176.4726	169.1285	179.1294	182.8042	199.3976
(% error)		(0.00)	(0.26)	(4.35)	(1.30)	(3.38)	(12.8)
δ	2.400000	2.400022	2.376536	2.348355	2.318193	2.285436	2.226665
(% error)		(0.09)	(0.98)	(2.15)	(3.41)	(4.77)	(7.22)
K_{11} (M^{-1})	25.00000	24.9998	25.21164	25.47061	25.75374	26.06845	26.65279
(% error)		(0.00)	(0.85)	(1.88)	(3.01)	(4.27)	(6.61)
K_{21} (M^{-1})	800.0000	800.0074	792.1785	782.7849	772.7311	761.8121	742.2218
(% error)		(0.00)	(0.98)	(2.15)	(3.41)	(4.77)	(7.22)

appears in the general shapes of the descending portion of solubility. Unlike the S_2L/S_2L-precipitate system, the curvature of this region actually increases with the magnitudes of K_{11}, K_{21} and K_{11}/K_{21} ratio as well as S_t, with no evidence for an inversion of the solubility to higher values with L_t as was seen before. This may become more obvious from an inspection of Figs. 6 and 7 which demonstrate how the concentrations of all soluble species vary over the entire scale of the phase diagrams for both systems. For the S_2L/S_2L-precipitate system shown in Fig. 6, both free solute [L] and soluble [SL] concentrations increase rather dramatically with L_t in region III as S_2L remains fixed. In contrast, the soluble S_2L-complex concentration actually decreases as [SL] remains fixed

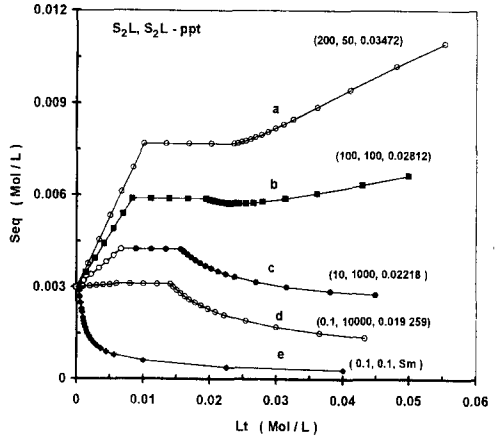

Fig. 4. Phase solubility diagrams of S_2L/S_2L-precipitate systems with different magnitudes of (K_{11}, K_{21}, K_{S21} and S_t) listed as such in parenthesis. a (200 M^{-1}, 50 M^{-1}, 4.1×10^{-8} M^3, 0.03472 M); b (100 M^{-1}, 100 M^{-1}, 3.8×10^{-8} M^3, 0.02812 M); c (10 M^{-1}, 1000 M^{-1}, 3.4×10^{-8} M^3, 0.02218 M); d (0.1 M^{-1}, 10000 M^{-1}, 2.8×10^{-8} M^3, 0.01926 M); e (0.1 M^{-1}, 0.1 M^{-1}, 2.7×10^{-8} M^3, 0.003002 M).

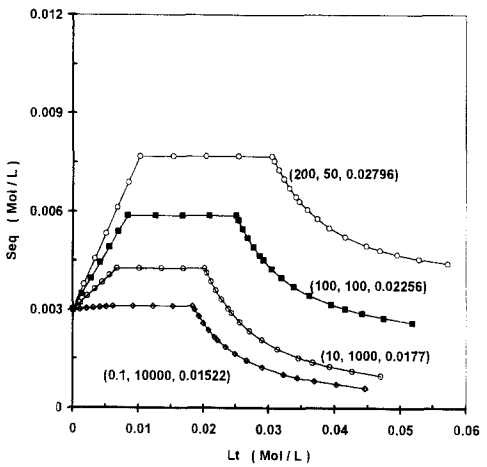

Fig. 5. Phase solubility diagrams of S_2L/SL-precipitate systems with different magnitudes of (K_{11}, K_{21}, K_{S11} and S_t) listed as such in parenthesis. a (200 M^{-1}, 50 M^{-1}, 1.36×10^{-5} M^2, 0.028 M); b (100 M^{-1}, 100 M^{-1}, 1.27×10^{-5} M^2, 0.023 M); c (10 M^{-1}, 1000 M^{-1}, 1.14×10^{-5} M^2, 0.0177 M); d (0.1 M^{-1}, 10000 M^{-1}, 9.24×10^{-6} M^2, 0.01522 M).

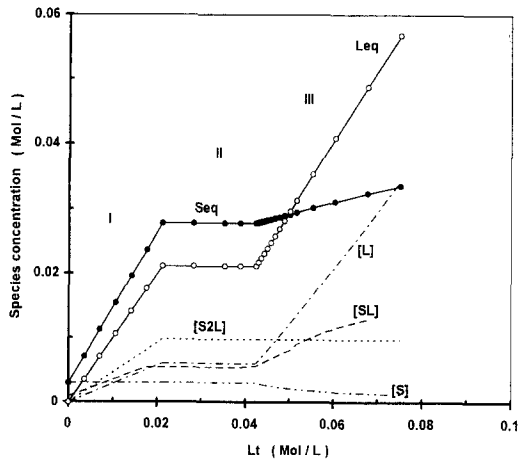

Fig. 6. A plot showing the variation of the molar concentrations of all soluble species against L_t for an S_2L/S_2L-precipitate system having the parameter values: $S_o = 0.003$ M, $S_m = 0.00562$ M, $L_m = 0.00834$ M, $L_p = 0.00159$ M, $[L_m] = 0.006$ M, $K_{11} = 300\ M^{-1}$, $K_{21} = 600.0\ M^{-1}$, $K_{S21} = 5.4 \times 10^{-7}\ M^3$ and $S_t = 0.02067$ M.

for the S_2L/SL-precipitate system depicted in Fig. 7. The magnitude of free solute concentration is so low in either case to have any significant balancing effect in comparison. The variation of concentrations of other soluble species with L_t over the entire range of the phase diagram is also shown in both figures. For the same values of S_o, S_t, K_{11} and K_{21}, the width of the plateau depends on the type of complex precipitate: it is higher for an SL- than an S_2L-complex precipitate.

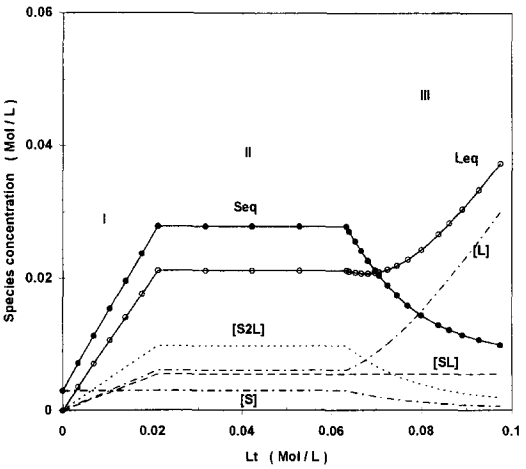

Fig. 7. A plot showing the variation of the molar concentrations of all soluble species against L_t for an S_2L/SL-precipitate system having the parameter values: $S_o = 0.003$ M, $S_m = 0.00562$ M, $L_m = 0.00834$ M, $L_p = 0.00159$ M, $[L_m] = 0.006$ M, $K_{11} = 300\ M^{-1}$, $K_{21} = 600.0\ M^{-1}$, $K_{S11} = 1.8 \times 10^{-5}\ M^2$ and $S_t = 0.02067$ M.

4. Conclusions

A set of simple relations has been developed to analyze for the first time the entire phase solubility diagrams of S_2L-type complexes to obtain individual partial formation and solubility product constants. Using the measured quantities S_o, S_m, L_m, L_p, S_{eq} and L_t, the descending portion of the diagram can for the first time be rigorously analyzed in terms of one floating parameter using standard nonlinear least squares. The model has been tested for both types of S_2L-phase diagrams, those having an S_2L-complex precipitate and others with an SL-complex precipitate, instead. Only two simple relations are involved in either case: Eqs. (29) and (30) in the former and Eqs. (40) and (41) in the latter case, as has been described in the discussion. Through simulation of experimental data with statistical random noise, it was shown that reasonable estimates of formation constants K_{11} and K_{21} may be obtained, provided the percent error in solubility measurements does not exceed 4% of the optimal solubility S_m. The variation of the general features of the phase diagrams with K_{11}, K_{21}, K_{S21} and S_t has been discussed for both types of systems. The observation of a rise following a decrease in the solubility of some compounds has been shown to occur in S_2L/S_2L-precipitate systems for which $K_{21} > K_{11}$ and not due to possible formation of higher order complexes. None of this occurs in systems in which an SL-complex precipitates leaving the S_2L-complex soluble. It has also been shown that the curvature of the descending portion is comparatively more steep for S_2L/SL-precipitate than S_2L/SL-precipitate systems. The solubility may become lower than the intrinsic solubility only for those systems in which an SL-complex precipitates. This model may be applied in the analysis of substrate-ligand complexes, including drug-cyclodextrin complexes, for which only the apparent formation constants have usually been obtained.

References

Abdul Rasool, A., Hussain, A.A. and Dittert, L.W., Solubility enhancement of some water-insoluble drugs in the presence of nicotinamide and related compounds. *J. Pharm. Sci.*, 80 (1991) 387–393.

Connors, K.A. and Pendergast, D.D., Microscopic binding constants in cyclodextrin systems: complexation of α-cyclodextrin with sym-1,4-disubstituted benzenes. *J. Am. Chem. Soc.*, 106 (1984) 7607–7614.

Connors, K.A., Lin, S. and Wong, A.B., Potentiometric study of molecular complexes of weak acids and bases applied to complexes of α-cyclodextrin with para-substituted benzoic acids. *J. Pharm. Sci.*, 71 (1982) 217–222.

Connors, K.A., Paulson, A. and Toledo-Velasquez, D., Complexation of α-cyclodextrin with sym-4,4′-disubstituted biphenyls. *J. Org. Chem.*, 53 (1988) 2023–2026.

Duchene, D. and Wouessidjewe, D., The current state of β-cyclodextrin in pharmaceutics. *Acta Pharm. Technol.*, 36 (1990) 1–6.

Higuchi, T. and Connors, K.A., Phase solubility techniques. *Adv. Anal. Chem. Instr.*, 4 (1965) 117–212.

Hoshino, T., Ishida, K., Irie, T., Hirayama, F. and Uekama, K., Reduction of photohemolytic activity of benoxaprofen by β-cyclodextrin complexations. *J. Inclus. Phenom.*, 6 (1988) 415–423.

Krishnamoorthy, R. and Mitra, A.K., Complexation of weak acids and bases with cyclodextrins: effects of substrate ionization on the estimation and interpretation of association constants. *Int. J. Pharm. Adv.*, 1 (1996) 329–343.

Liu, F., Kildsig, D.O. and Mitra, A.K., β-Cyclodextrin/steroid complexation: effect of steroid structure on association equilibria. *Pharm. Res.*, 7 (1990) 869–873.

Marques, H.M.C., Hadgraft, J. and Kellaway, I.W., Studies of cyclodextrin inclusion complexes. I. The salbutamol-cyclodextrin complex as studied by phase solubility and DSC. *Int. J. Pharm.*, 63 (1990) 259–266.

Maurin, M., Rowe, S.M., Koval, C. and Hussain, M., Solubilization of nicardipine hydrochloride via complexation and salt formation. *J. Pharm. Sci.*, 83 (1994) 1418–1420.

Menard, F.A., Dedhiya, M.G. and Rhodes C.T., Physicochemical aspects of the complexation of some drugs with cyclodextrins. *Drug Dev. Ind. Pharm.*, 16 (1990) 91–113.

Muller, B.W. and Brauns, U., Solubilization of drugs by modified β-cyclodextrins. *Int. J. Pharm.*, 26 (1985) 77–88.

Seo, H., Tsuruoka, M., Fujinaga, T., Otagiri, M. and Uekama, K., Enhancement of oral bioavailability of spironolactone by β- and γ-cyclodextrin complexations. *Chem. Pharm. Bull.*, 31 (1983) 286–291.

Sideris, E.E., Valsami, G.N., Koupparis, M.A. and Macheras, P.E., Determination of association constants in cyclodextrin/drug complexation using the scatchard plot: application to β-cyclodextrin-anilinonaphthalenesulfonates. *Pharm. Res.*, 9 (1992) 1568–1574

Streng, W.H., Hsi, S.K., Helms, P.E. and Tan, H.G.H., General treatment of pH-solubility profiles of weak acids and bases and the effects of different acids on the solubility of a weak base. *J. Pharm. Sci.*, 73 (1984) 1679–1684.

Takahashi, T., Kagami, I., Kitamura, K., Nakanishi, Y. and Imasato, Y., Stabilization of AD-1590, a non-steroidal antiinflamatory agent in suppository bases by β-cyclodextrin complexation. *Chem. Pharm. Bull.*, 34 (1986) 1770–1774.

Tong, W., Lach, J.L., Chin, T. and Guillory, J.K., Microcalorimetric investigation of the complexation between 2-hydroxypropyl-β-cyclodextrin and amine drugs with the diphenylmethyl functionality. *J. Pharm. Biol. Anal.*, 9 (1991) 1139–1146.

Uekama, K., Ikeda, Y., Hirayama, M., Otagiri, M. and Shibata, M., Inclusion complexation of *p*-hydroxybenzoic acid esters with α- and β-cyclodextrins: dissolution behaviors and antimicrobial activities. *Yakugaku Zasshi*, 100 (1980) 994–1003.

Valsami, G.N., Macheras, P.E. and Koupparis, M., Binding studies of ions with cyclodextrins using ion-selective electrodes. *J. Pharm. Sci.*, 79 (1990) 1087–1094.

Yusuff, N. and York, P., Spironolactone-cyclodextrin complexes: phase solubility and ultrafiltration studies. *Int. J. Pharm.*, 73 (1991) 9–15.